45TH TURBOMACHINERY & 32ND PUMP SYMPOSIA
HOUSTON, TEXAS | SEPTEMBER 12 – 15, 2016
GEORGE R. BROWN CONVENTION CENTER

COUPLING GUARD TEMPERATURE AND WINDAGE POWER LOSS: CFD ANALYSIS AND EXPERIMENTS

Adam Thompson
Mechanical Engineer
John Crane
Manchester, Greater Manchester, UK
adam.thompson@johncrane.com

Tianbo Zhai
Research Assistant
Texas A&M University
College Station, Texas, USA
zhaitb@tamu.edu

Alan Palazzolo
Professor
Texas A&M University
College Station, Texas, USA
a-palazzolo@tamu.edu

Amir Keshmiri
Associate Professor
Manchester Metropolitan University
Manchester, Greater Manchester, UK
a.keshmiri@mmu.ac.uk

Adam Thompson is a Mechanical Engineer working in the coupling engineering team at John Crane. He has over nine years of experience working in industrial product design, and research and development roles. He is involved in the design and development of existing coupling product ranges and bespoke coupling solutions for customers, technical support and delivering training to a global audience. Mr. Thompson obtained a First Class Bachelor's degree and Master's degree with Distinction in Mechanical Engineering, from the Manchester Metropolitan University, UK, and is registered as a Chartered Engineer with the IMechE.

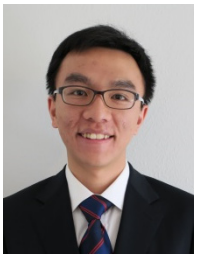

Tianbo Zhai is a Mechanical Engineering student currently pursuing his MS degrees at Texas A&M University, under the supervision of Dr. Alan Palazzolo. His research includes Computational Fluid Dynamic simulation of coupling guard heating and gearbox windage power loss, where he collaborated with industry partners and conducted several case studies. He also has multiple project experience in design and manufacturing. Mr. Zhai received his Bachelor's degree in Mechanical Engineering from Harbin Institute of Technology, Harbin, China.

Dr. Alan Palazzolo is a Professor of Mechanical Engineering at Texas A&M University and received his MS and PhD degrees from the University of Virginia. He is an endowed Texas A&M Engineering Station (TEES) professor, an ASME Fellow, an R&D 100 Award Recipient, has published 70 archival journal articles and has received numerous internal awards in teaching and scholarship. His active research areas include rotordynamics, seal and bearing forces, flywheel energy storage, coupling and gear heating, motor induced vibrations, desalination, wind turbines and flow in heart pumps.

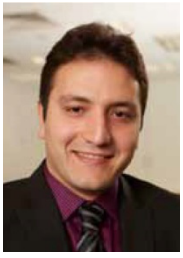

Dr. Amir Keshmiri is an Associate Professor in Fluid Mechanics at Manchester Metropolitan University (MMU), and received his BEng, MSc and PhD from the University of Manchester. Dr. Keshmiri is a Chartered Engineer (CEng) and the Deputy Director of the 'Engineering and Materials Research Centre' at MMU. He has over 10 years of experience in Computational Fluid Dynamics and has published over 30 journal and conference papers in the area of turbulence modeling, heat transfer, nuclear thermal hydraulics and more recently biomedical engineering. He is also the recipient of numerous awards and honors for his research and teaching in the above areas.

ABSTRACT

High temperatures inside coupling guards can cause machinery down time and loss of revenue. As a result, many industries invest significant time and effort trying to reduce heat generation. Windage flanges are a standard feature on high performance couplings with the purpose of reducing heat generation within guards. However, previous testing and Computational Fluid Dynamic (CFD) simulation carried out by Pennington and Meck (2012) have cast doubt on the effectiveness of this feature. The forthcoming fifth edition of API 671 is expected to reduce the maximum allowable guard temperature from 160°F (70°C) to 140°F (60°C), to reduce the risk of irreversible surface contact burns. In order to comply with the API requirement, it is important to understand how features such as windage flanges and radial guard clearance affect heat generation.

CFD analysis and physical testing are presented in this paper. Improvements to the test configuration setup have been made to achieve increased coupling surface speeds of 175m/s (compared to 123m/s in previous testing by Pennington and Meck (2012)), and simplified to isolate the effects of the windage flange. This paper investigates the effectiveness of windage flanges, as well as the effect of guard radial clearance on heat generation inside coupling guards, and resultant coupling guard temperature, at much higher speeds than in previous studies.

In total, six test configurations were simulated, consisting of two test couplings (with and without windage features) tested with three different sized coupling guards, creating variable radial clearances. CFD analysis results conclude that the windage flange features are ineffective in reducing heat generation inside the guard, and coupling guards with a larger radial clearance result in lower temperatures inside the guard. However, this approach is less effective above a guard radial clearance of 40mm, after which the windage flange has little effect on the temperature within the coupling guard. In addition, temperature results from the validated CFD model were found to be within 4 percent of the physical experimental data.

INTRODUCTION

Couplings are mechanical devices used to transfer power (torque and speed) between the rotating shafts of two machines (driver and driven), whilst allowing for some misalignment between the shafts. High performance metal membrane couplings, shown in Figure 1, are designed for special applications, predominantly involving large Turbomachinery which operate at high speeds.

Figure 1. High Performance HSFE Coupling (Courtesy of John Crane)

Coupling enclosures (Figure 2) are often oil tight guards often fitted by the vendor for safety reasons so that during operation of the drive train, personnel cannot gain access to the rotating parts (American Petroleum Institute, 2007), and to prevent a fire hazard by trapping any oil escaping from the machinery and returning it back to an oil reservoir (Calistrat, 1990).

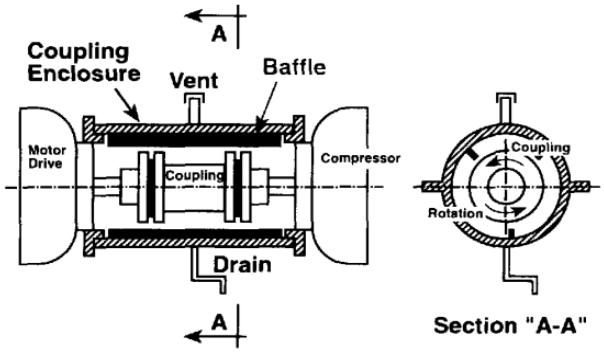

Figure 2. Coupling Enclosed in a Coupling Enclosure (Carter, et al., 1994)

Coupling guards were successfully used with oil lubricated couplings (e.g. gear coupling) for decades due to the lubrication providing a cooling effect. However, the replacement of these with dry metal membrane couplings resulted in significant heat generation within the guard during drivetrain operation (Calistrat and Munyon, 1985). A possible solution is to leave the old oil spray system in place and activate it when the guard temperature becomes a problem. However, maintaining coupling temperature in this way results in continued control and support of the lubrication system, eliminating one of the advantages of a dry metal membrane coupling, zero maintenance. The current 4th edition of API 671 states maximum allowable guard temperature is 160°F (70°C), however this is expected to reduce to 140°F (60°C) in the forthcoming 5th edition. This reduction is an effort to improve safety, as ASTM C1055 (Standard Guide for Heated System Surface Conditions that Produce Contact Burn Injuries) recommends the average person can touch a surface at a temperature of 140°F (60°C) for five seconds without sustaining irreversible burn damage (ASTM International, 2014).

Carter, et al., (1994) state that the main contributor to this heat generation is the shearing of the air and air turbulence inside the guard (i.e. windage), both caused by friction between the rotating coupling and the air inside the guard. Friction is caused by the adjacent layers of air rotating at different speeds within the coupling guard. Dissimilar diameters of a coupling can generate further heat due to face friction inducing a circular motion of air flow (Calistrat and Munyon, 1985). Turbulence is generated by the fasteners that connect the coupling components as they rotate at high speed within the guard, churning the air stream (Calistrat and Munyon, 1985).

Heat generation from couplings as a result of windage is waste energy, also known as churning losses. Excessively high temperatures within coupling guards caused by high churning losses is unsafe and can cause machine failure resulting in downtime (Calistrat, 1990), loss of revenue and possible litigation fees. Due to the negative effect of high churning losses, many industries invest significant time and effort in order to reduce them (Pennington and Meck, 2012).

Exposed bolts and nuts, particularly those installed at larger diameters have been identified as being the main contributor towards windage generation (Calistrat, 1990). A method of reducing windage is to machine specially designed anti-windage features called ‘windage flanges’. Windage flanges aim to reduce the churning of the air produced by rotating coupling drive bolts, by shielding them, to an extent, from the surrounding air particles (Figure 3). However, previous test work and CFD simulation carried out by Pennington and Meck (2012) have cast doubt on the effectiveness of this feature.

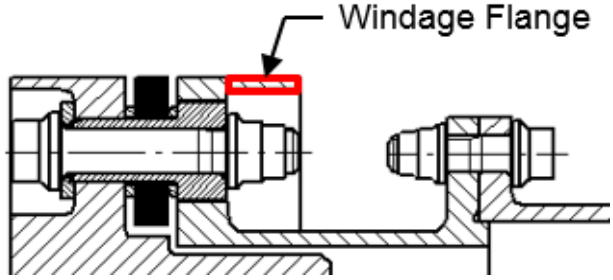

Figure 3. Section View from a High Performance Coupling Highlighting a Windage Flange

Pennington and Meck (2012) state that as a result of previous studies, anti-windage features are recognized as an integral part of high performance coupling design, which aims to reduce the churning losses and heat generated by the coupling. These features are difficult to manufacture and increase the complexity of coupling assembly by obscuring the access of tooling to the drive bolts. In addition they can lead to stress concentrations at flange intersection points which can lead to fatigue failure (Pennington and Meck, 2012). All these factors greatly increase the cost associated with the coupling.

Pennington and Meck (2012) concluded that windage features are not as efficient as generally believed and their results strongly suggested that they fail to make a significant impact on reducing churning losses and coupling guard temperatures. Pennington and Meck (2012) propose that one reason is that although the CFD results show that the addition of a windage flange reduced the flow separation at the coupling bolts by a small amount, the additional surface area of the feature caused shearing of the air which in turn eliminated any net gain.

Previous testing by Pennington and Meck (2012) involved many variables, making drawing definite conclusions from the results difficult. Testing carried out in this study focuses on two variables only; the presence of the windage flange feature, and the radial guard clearance, in order to isolate the effect that they have on temperature within the guard.

In addition, although physical testing by Pennington and Meck (2012) was planned to be carried out at a rotational velocity of 10,000rpm (175m/s surface speed), due to vibration problems test speeds of only 7,000rpm (123m/s surface speed) were managed. This did not generate enough surface speed on the coupling outside diameter (OD) to obtain high differential churning loss results from comparative coupling tests. Results for CFD testing given by Pennington and Meck (2012) as shown below in Figure 4, show that the rate of churning losses greatly increases above speeds of 7,000rpm (123m/s surface speed) which generate approximately 4hp of churning losses, to 10,000rpm (175m/s surface speed) which generate approximately 11hp (increased by a factor of approx. 3).

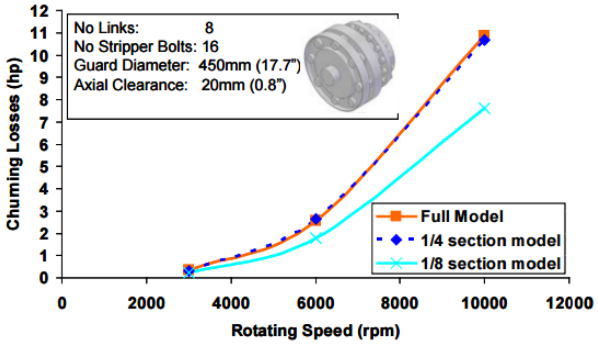

Figure 4. Churning Loss Prediction vs. Rotating Speed (Pennington and Meck, 2012)

In this study, physical testing was redesigned to achieve a coupling surface speed of 175m/s in order to generate increased churning losses and magnify differences in comparative test results. The increased test speeds not only aid in the analysis of results, but also allow for more accurate CFD model validation since at these speeds churning losses are much more sensitive to changes in input conditions. In addition, by varying radial guard clearance (small: 20mm; medium: 40mm; large: 60mm), parametric studies can be conducted and this will provide more cases for CFD validation and helps develop a more robust CFD model for end users to predict coupling guard temperature and windage power loss.

If windage flanges are proved ineffective in reducing heat generation, as well as the safety benefits and conformance to API 671 requirements, removing them has huge potential to reduce churning losses, increase energy efficiency and reduce customers' energy costs in relation to rotating Turbomachinery. In addition, there is possible scope to reduce coupling manufacturing costs significantly if the windage flanges are found to be ineffective.

The main aim of this study is to determine the effectiveness of windage flanges and the influence of coupling to guard radial clearance on heat generation inside coupling guards, in realistic operating conditions via CFD analysis and physical testing. Testing is to be carried out at higher test speeds than in previous studies, in order to generate increased churning losses and magnify differences in comparative test results. A secondary aim of this study is to create a CFD model with temperature results that closely match the physical test results, in order to work towards more accurate simulation and prediction of coupling guard temperature for design optimization.

PROCEDURE

ANSYS CFX is a powerful CFD code used for the simulation and analysis of fluid flow within virtual environments. Steady state analysis with conjugate heat transfer was carried out in this study using ANSYS CFX Version 15.0.7. A mesh was generated and a model set up to simulate fluid flow around the test coupling rotating at high speed within the stationary coupling guard, this was carried out for all six test configurations as listed in Table 1.

Table 1. Physical Test Configurations

NO. OF TEST CONFIGURATION	WINDAGE FLANGE (YES or NO)	SIZE OF COUPLING GUARD
1	Yes	Small
2	No	Small
3	Yes	Medium
4	No	Medium
5	Yes	Large
6	No	Large

Test configuration 5 was physically tested on the dynamic test rig and used to validate the CFD model. The remaining CFD models were set up as per the validated model. Physical testing of the remaining test configurations is planned to be carried out in order to further assess the accuracy of the CFD models, in an effort to create a model setup philosophy that can be used for predicting guard temperature.

Test Rig Overview

The test rig setup for the non-windage coupling with medium guard configuration is shown in Figure 5 (guard cylinders removed for viewing purposes). The test rig capability allowed for a surface speed of 175m/s to be reached on the test coupling OD. Two annulus plates were mounted onto the stationary housing of the test rig, together with the diameter-variable cylinder halves that make up the coupling guard. The cylinder halves allowed for a variable radial clearance from the coupling OD to the guard ID of 20mm, 40mm and 60mm.

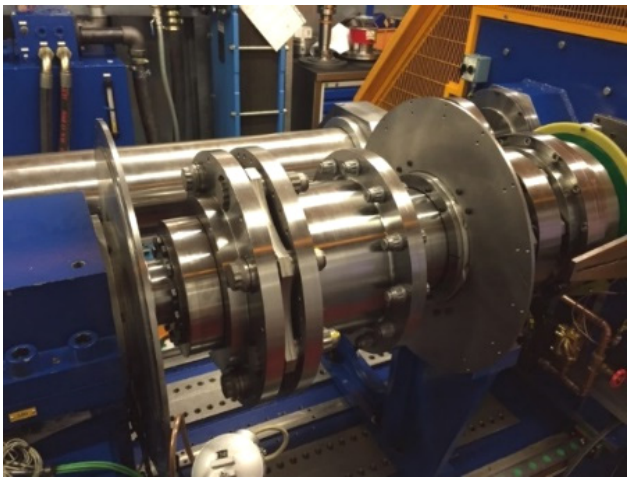

Figure 5. Test Rig Overview showing Test Configuration 4, Coupling without Windage Flanges with Medium Guard (Guard Cylinders Removed)

Temperature and pressure within the guard were measured by strategically placed thermocouples and pressure transducers installed in the coupling guard cylinders. The location of the thermocouples and pressure transducers (Figure 6) were determined from initial CFD

analysis which located hotspots within the guards. Hotspots are a desirable location for measurement points as they show areas of maximum change during the test which allows for differences between comparable models to be magnified when analyzing results. During physical testing the test rig was run at the specified test speed of 7,500 rpm until steady state temperature in the guard was reached and held to within +/- 0.1°C for an hour (approximately 8 hours), at which point the values for all measurement devices were recorded and the test ended.

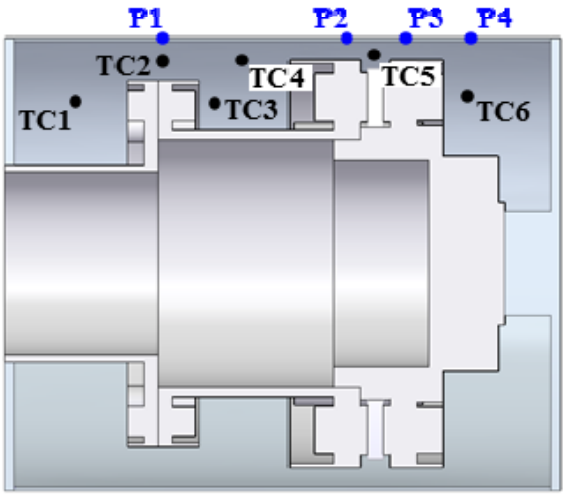

Figure 6. Measurement Probe Locations in Physical Test Setup
Thermocouple (TC1 to TC6) and Pressure Transducer (P1 to P4)

Coupling Geometry

As the dynamic test rig had certain spatial restrictions, in order for the test coupling to fit into the rig and achieve surface speeds on the coupling OD of 175m/s, a hybrid version of a high performance coupling was specially designed and manufactured. One half (the test half) is larger in order to achieve the circumferential speed on the OD, and the other half is smaller so as not to clash with the rig. Again, due to space restrictions, the guard had to intersect the test coupling halfway along the length of the spacer component. Figure 7 shows the coupling geometry with the testing domain highlighted, which is defined by the size of the guard.

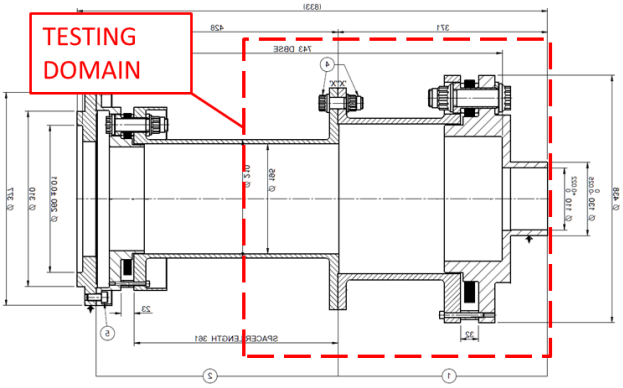

Figure 7. Cross-sections of Test Coupling without
Windage Feature with Test Domain Highlighted

Computational Domain and Mesh

To capture turbulence and heat transfer effects, the k-ω shear stress transport (SST) turbulence model and energy equation model were selected. In order to reduce computational time, and aid solution convergence within CFX, a number of simplifications were made to the coupling and guard assembly to remove any unnecessary complex geometry, which added no value to the simulation. In addition,

a separate study by Pennington and Meck, (2012) who used a similar method of CFD analysis on a coupling, confirmed that although geometric symmetry exists down to a model size of a 1/8 section of the coupling, flow around the coupling is only symmetrical and computed correctly down to a model size of a 1/4 section of the coupling. Therefore, the model size was reduced to a 1/4 section of the full model and periodic boundary conditions were employed, in order to reduce computational time (Figure 8).

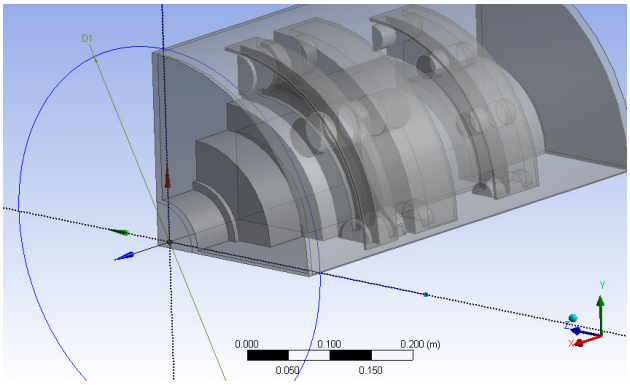

Figure 8. Schematic of 1/4 Section Computational Model (created in ANSYS Design Modeller)

The mesh was generated with four domains in order to reflect realistic physical conditions, as illustrated Figure 9. There are two fluid domains, which model the fluid in-between the coupling and guard (shroud), and the fluid inside the coupling. Due to the complex geometry and expected turbulence of the model, a hybrid tetrahedral mesh was created which incorporated a finer density in the narrow intricate regions of the model, coarser density in the larger fluid and solid regions, and inflation layers around all fluid regions. A mesh independency study was carried out on one model after the CFX setup was complete in order to finalize mesh element sizing and to ensure adequate mesh accuracy. The material in the fluid domains was set to air, with the density specified as 'ideal gas' for simplicity (follows ideal gas law). The rotating coupling domain and stationary guard domain are modeled which allows for full heat transfer analysis of the solid bodies. The material for the solid bodies was set to carbon steel and the thermal conductivity modified to reflect carbon steel at the estimated final temperature (thermal conductivity is temperature dependent).

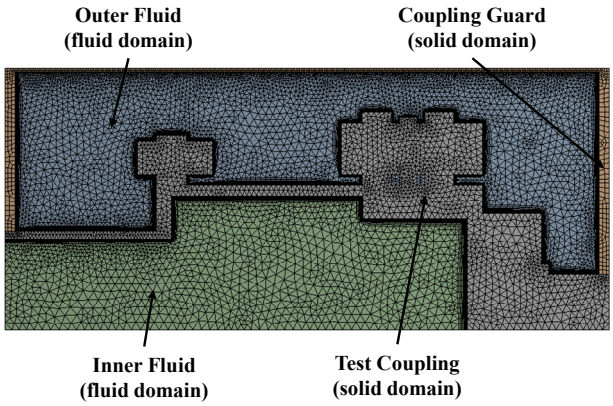

Figure 9. Mesh Model Section showing Four Domains, for Medium Size Guard without Windage Flanges (in ANSYS Meshing)

Boundary conditions were imposed within CFX to reflect the physical conditions as closely as possible. Since the inner-fluid domain is connected with the other side of the spacer, outside of the test domain (not shown in the figure), the air in the hollow of the coupling must be free to flow in or out of the domain. Therefore, an opening boundary condition with 140°F (60°C) inlet air temperature was imposed at this location. In addition, as a result of recorded test data, a steady state temperature of 140°F (60°C) was also set on the right guard face to represent the temperature of the shaft. Thermal boundary conditions on both sides of the guard were assumed to be constant at a temperature of 160°F (70°C). This is due to the test rig housing and shaft temperature having an influence on the temperature of the guard.

Significant heat is dissipated by natural convection through the coupling guard to atmosphere, and it is therefore crucial to determine the heat transfer coefficient of the guard solid body accurately, as the temperature inside the guard increases. Assuming that the natural convection of the coupling guard resembles that of a horizontal cylinder, after some manipulations the correlation below was derived. The heat transfer coefficient was then imposed as a function of the temperature difference within the CFX-Pre setup.

$$\bar{h} = 1.39(T_s - T_\infty)^{0.333} \tag{1}$$

where

$\bar{h}$ Heat transfer coefficient (W/m^{2}K)

T_s Volume average temperature of coupling guard (K)

T_∞ Ambient temperature (K), set at 80°F (27°C)

A summary of the boundary condition details imposed on the model is illustrated in Figure 10.

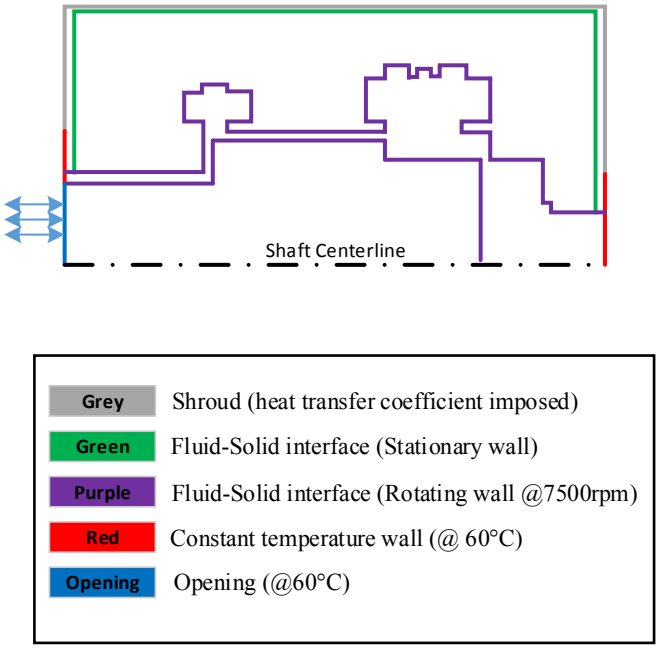

Figure 10. Boundary Conditions Imposed on the CFD Model

Solid models of all six test configurations were built for the test coupling (with and without windage features) with variable radial clearances of 20mm, 40mm and 60mm as shown in Figure 11. Simulations of all six models were run until the solution was deemed to have converged, approximately 3000 iterations. Convergence was determined when residual values were deemed to be sufficiently small (less than 0.0001), and monitored volume averaged temperature results remained at a constant amplitude.

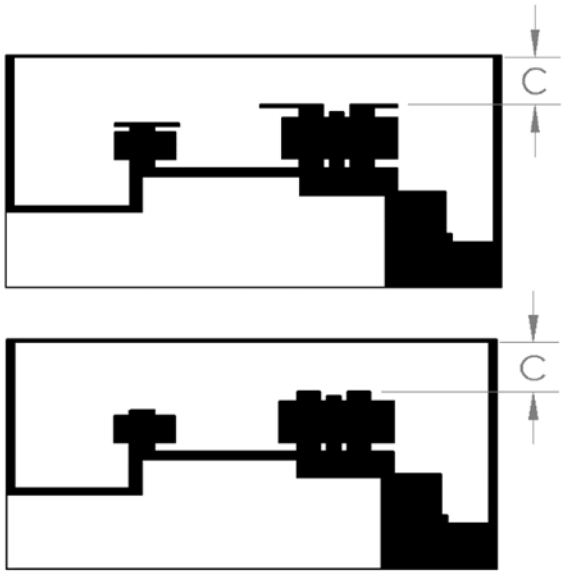

Figure 11. Radial Clearances of Coupling Guard (C=20mm, 40mm and 60mm)

RESULTS AND DISCUSSION

Validation and Analysis of CFD Simulation Result against Physical Test Results

Medium Guard Test Configuration 4

The CFD model based on test configuration 4 was built and the following temperature (with 2D streamline overlay) and pressure plots were generated in ANSYS CFD-Post. The simulation results shown in Figure 12 show that the temperature range within the guard is between 141°F – 245°F (61°C – 118°C), with the higher temperatures located in an area along the full length at the top of the guard. The streamline plot shows that large circulation patterns distribute air from the large coupling OD along the full length of the guard to the left and right guard faces.

Air circulation within the guard enhances turbulence and mixing of the air, subsequently heating or cooling the surrounding air. Figure 13 shows that the hottest part of the coupling is located at the large diameter flanges, and therefore the observed circulation patterns allow for this heat to be circulated effectively along the full length of the top area of the guard, giving a uniform temperature band along this area. It can be seen that the areas in the guard closer to the coupling do not reach the same temperature as at the OD, and that a uniform temperature within the entire inner-guard in not achieved. The streamline plot shows that this is due to the air flow circulation not extending into these areas, due the reduced mixing in this area, a temperature variation within the guard remains.

In addition, the air circulation patterns observed could be further stimulated by the temperature of the coupling (Figure 13). The large diameter coupling flanges, which are the hottest part of the coupling at 230°F (110°C), cause air to heat up and rise to the outer diameter of the coupling guard. At the same time, the left and right sides of the coupling are cooler at 140°F (60°C) and cool the air causing it to fall and drop to the inner diameter of the guard. This heating at the large coupling OD and cooling at the coupling edges could aid in inducing the two main circulation patterns observed.

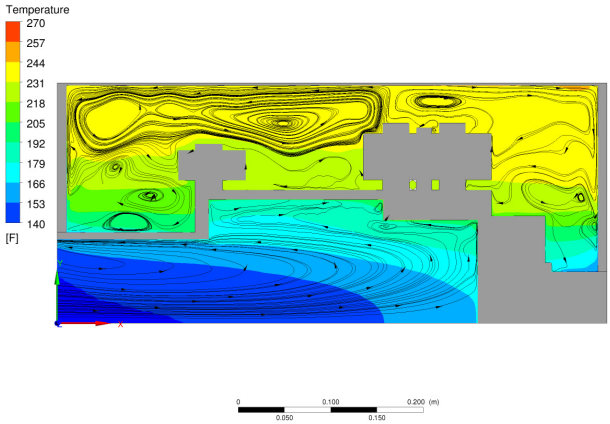

Figure 12. Temperature Contour Plot with 2D Streamline Overlay (Fluid Domain) for Configuration 4: Medium Size Guard without Windage Flanges

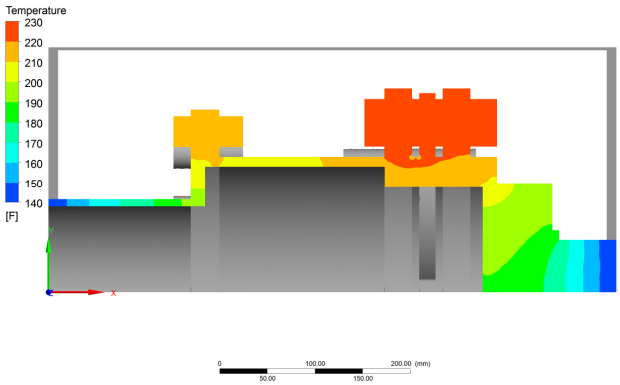

Figure 13. Coupling Temperature Contour Plot (Solid Domain) for Configuration 4: Medium Size Guard without Windage Flanges

The pressure contour was plotted as shown in Figure 14, with the values given being relative to an atmospheric pressure of 14.7psi (1bar). Analysis of the pressure distribution within the guard shows a pattern from negative pressure, -1.2psi (-83mbar) close to the coupling, to positive, 0.1psi (7mbar) at the guard face, with the pressure only turning positive near the guard surface. This supports the notion of a negative pressure vacuum effect that can be present on large diameter couplings rotating at high speed as discussed by Carter, et al. (1994). They state that large diameter couplings naturally have a higher surface speed that can centrifuge air radially outwards away from the shaft, creating a negative pressure zone that can suck oil past labyrinth seals. During physical testing for this test configuration, this phenomenon was directly experienced, with large amounts of oil being sucked out of an adjoining labyrinth seal. To rectify this, a floating ring separation seal was designed and installed, to create and maintain a positive pressure in the labyrinth ID region.

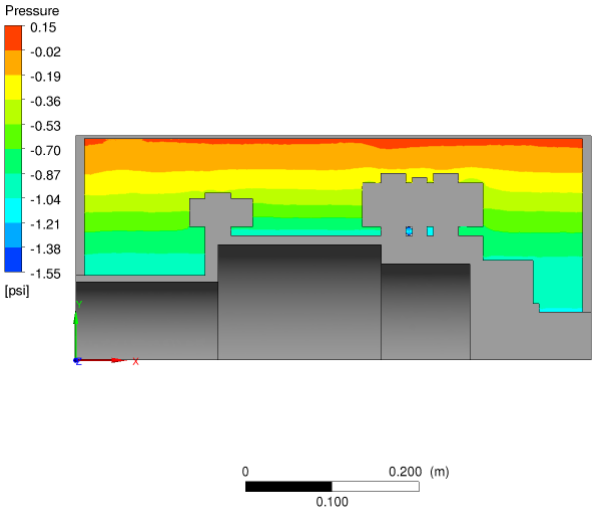

Figure 14. Pressure Contour Plot (Fluid Domain) for
Configuration 4: Medium Size Guard without Windage Flanges

A one-on-one comparison between simulation results and physical test data is shown below in Table 2 and Figure 15. The close match between experimental and simulation data (<4 percent), and analysis of the plots above, validate that the current CFD model setup is accurate and therefore justifies the decision to model the remaining configurations based on similar procedures.

Table 2. Comparison between Test and Simulated Results for Test Configuration 4

No. of Thermocouple	**Location (in CFD Model)**			**Medium Guard, Non-windage Features**		***Percent Difference***
	X / mm	***Y / mm***	***Z / mm***	***Test Data/ °C (+/- 0.1°C)***	***Predicted Temperature/ C°***	
TC 1	*77*	*172*	*0*	*112.1*	*108.8*	*-3.0%*
TC 2	*169*	*228*	*0*	*116.1*	*113.3*	*-2.5%*
TC 3	*225*	*169*	*0*	*115.5*	*107.1*	*-7.2%*
TC 4	*339*	*239*	*0*	*119.6*	*113.4*	*-5.2%*
TC 5	*397*	*234*	*0*	*117.4*	*115.9*	*-1.3%*
TC 6	*495*	*177*	*0*	*116.1*	*112.7*	*-2.9%*
			Average	***116.1***	***111.9***	***-3.6%***

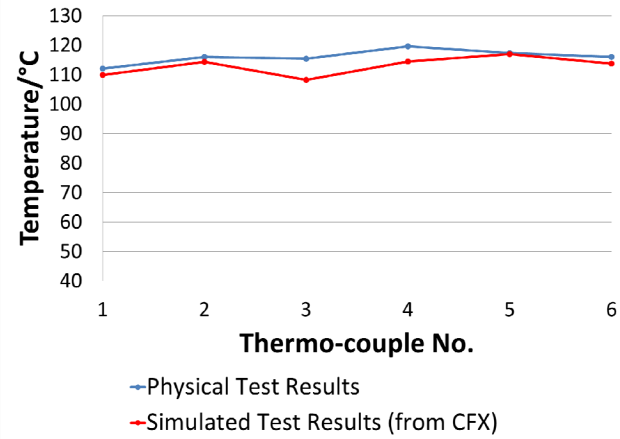

Figure 15. Plot of Comparison between CFX Simulation Results and Physical Test Results for Test Configuration 4, Medium Guard without Windage Flanges

CFX Results Analysis

Medium Guard Test Configuration 3

The CFD models based on the remaining test configurations were built and similar temperature (with 2D streamline overlay) and pressures plots generated in CFD-POST as shown below. From Figure 16, it can be seen that even though windage flanges were added, the temperature within the coupling guard was not reduced. The temperature within the guard was found to be between 141°F – 257°F (60°C – 125°C) which shows that the maximum temperature has increased by 12°F (7°C), and this was also reflected on the increase of guard temperature. The distribution of the temperature is not as uniformly mixed along the top area of the inner-guard. There is a larger area of high temperature above and to the right of the large coupling OD, and a thinner band of high temperature extending to the left of the guard. The 2D vector plots show that the air circulation in the guard, changes with the addition of the windage flanges. The large circulation pattern to the left is cut short to some extent by the windage flange geometry, and is not able to circulate heat generated by the windage flanges to this area as effectively. In addition, the larger windage flanges have resulted in significant disruption to the flow above them by splitting the main recirculation ring into several smaller ones with less turbulent kinetic energy.

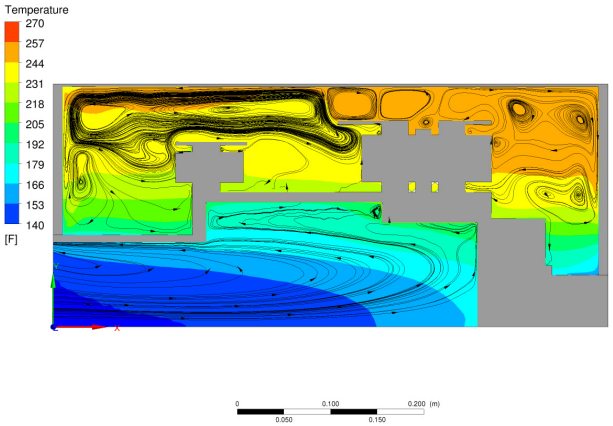

Figure 16. Temperature Contour Plot with 2D Streamline Overlay (Fluid Domain) for Configuration 3: Medium Size Guard with Windage Flanges

It should be noted that the higher temperature within the guard is due to the increased temperature of the coupling flanges (+15°F on large flanges) as shown in Figure 17. As the only change to the test configuration is the addition of the windage flanges, this must be the cause of the increased flange temperature. The root cause of this will be discussed later on in the paper.

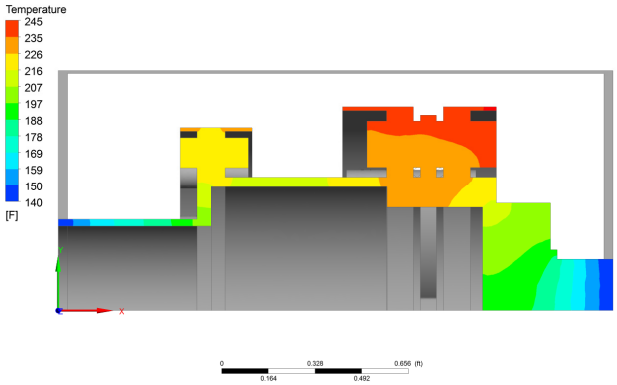

Figure 17. Coupling Temperature Contour Plot (Solid Domain) for Configuration 3: Medium Size Guard with Windage Flanges

The addition of windage flanges did not have any significant effect on the pressure within the guard as shown by Figure 18. The simulation results from the medium sized guard test configurations, therefore confirm that the windage flanges fail to reduce temperature within the guard, but instead result in an increase of temperature of 12°F (7°C).

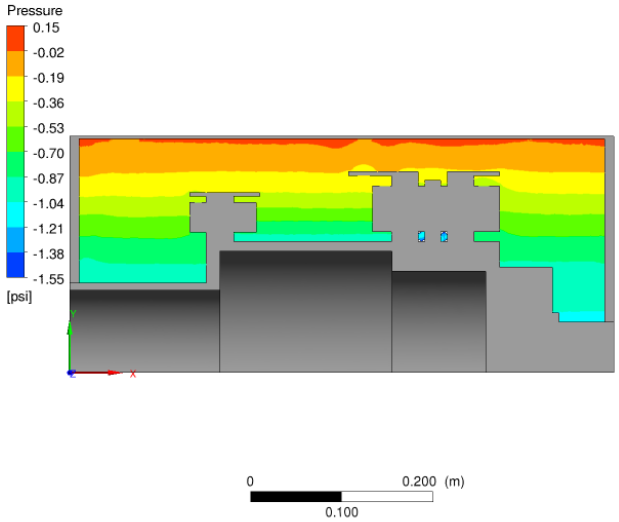

Figure 18. Pressure Contour Plot (Fluid Domain) for Configuration 3: Medium Size Guard with Windage Flanges

Small Guard Test Configurations 1 and 2

When the radial clearance of the guard is decreased from 40mm (medium size guard) to 20mm (small size guard), an increase in maximum temperature of 18°F (10°C) is observed, as shown in Figure 19. Analysis of the coupling temperature distribution showed the same behavior as that observed with the medium guard configurations, with the highest temperature present at the large coupling OD, which increased with the addition of windage flanges.

The 2D streamline plot in Figure 19 shows similar air circulation patterns to those found in the equivalent medium guard configurations plot, but with a more compressed and exaggerated flow circulation above and to the right of the large coupling OD. This seems to be resulting in a higher temperature more concentrated in this area.

Analysis of the pressure within the guard showed a similar distribution to that found in the equivalent medium guard configurations plot, but with a slightly increased pressure at the guard wall directly above the large coupling OD. This increase is only 0.02psi (1.4mbar) and is therefore classed as insignificant, and has no effect on the overall temperature of the guard. The minimum pressure within the distribution can be seen to have decreased from -1.5psi (103mbar) to -1.0psi (-69mbar). This shows that as the guard radial clearance increases, the negative pressure vacuum effect also increases.

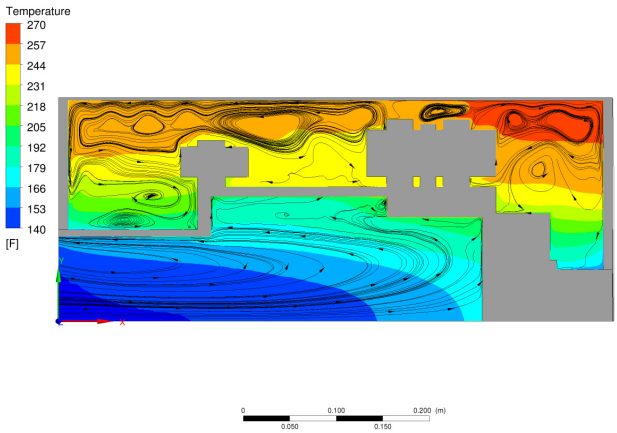

Figure 19. Temperature Contour Plot with 2D Streamline Overlay (Fluid Domain)
for Configuration 2: Small Size Guard without Windage Flanges

A higher temperature occurs again with the presence of the windage flange as shown below in Figure 20, but this time the increase is slightly less (7°F (4°C)) than that found with the medium guard configurations. The streamline plots (Figure 19 and Figure 20) show the reason for this is the same as found on the medium guard test configurations; the air circulation pattern to the left is being cut short by the windage flange geometry. The addition of windage flanges does not result in any significant change in the pressure within the guard.

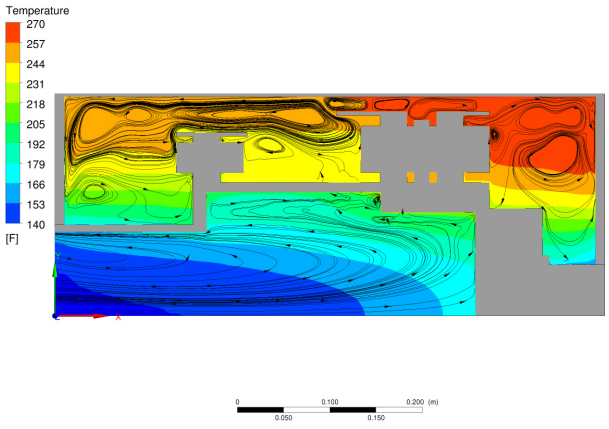

Figure 20. Temperature Contour Plot with 2D Streamline Overlay (Fluid Domain)
for Configuration 1: Small Size Guard with Windage Flanges

The simulation results from the small sized guard test configurations therefore confirm that the windage flanges again fail to reduce temperature within the guard, but instead result in an increase of temperature of 7°F (4°C). A reduction in the guard radial clearance

from 40mm to 20mm, results in an increase of maximum temperature within the guard of 18°F (10°C), and an increase in the negative pressure vacuum affect.

Large Guard Test Configurations 5 and 6

After increasing the radial clearance of the guard from 40mm (medium size guard) to 60mm (large size guard), there is no significant change in the maximum temperature in the guard, for the model without windage flanges (1°F increase). The 2D streamline plot shows very similar circulation patterns to those in the equivalent medium guard configuration which would explain the above observation to some extent.

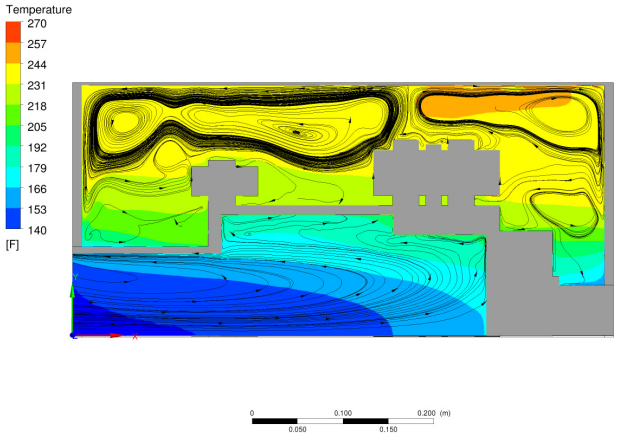

Figure 21. Temperature Contour Plot with 2D Streamline Overlay (Fluid Domain)
for Configuration 6: Large Size Guard without Windage Flanges

The pressure within the guard was found to have a similar distribution from negative pressure at the ID, to positive at the OD. However, the minimum pressure within the distribution can be seen to have decreased from -1.5psi (103mbar) to -1.2psi (-83mbar). This shows that as the guard radial clearance increases from 40mm to 60mm, the negative pressure vacuum effect decreases.

Combining the above observation with the results from the medium to small radial guard clearance, Figure 22 shows that the negative pressure vacuum effect increases from 20mm up to a point between 40 and 60mm, when it decreases again.

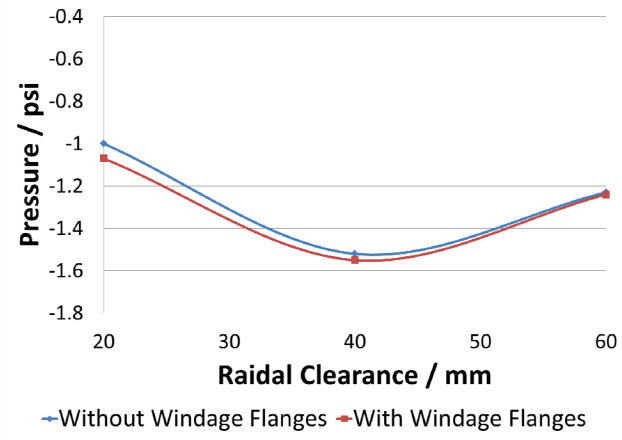

Figure 22. Negative Pressure Vacuum
Effect (inside guard) with Respect to Guard Radial Clearance

Figure 23 shows that, for the model with windage flanges, there is a decrease in maximum temperature inside the guard of 9°F (5°C),

when compared to the equivalent medium guard configuration results in Figure 16. The streamline plots no longer have the small circulation patterns above the large coupling OD windage flange. These have now been extended into larger flow patterns as on the windage model shown by Figure 21. This difference may explain why there is still a decrease in maximum temperature in this model when the radial clearance is increased, and not in the model without windage flanges which had no significant change observed.

In addition, adding windage flanges does not result in any significant change to the temperature or pressure inside the large guard.

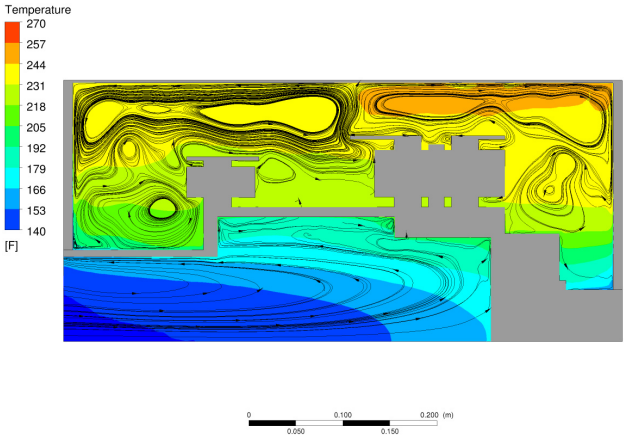

Figure 23. Temperature Contour Plot with 2D Streamline Overlay (Fluid Domain)
for Configuration 5: Large Size Guard with Windage Flanges

Results for the large guard configurations again show that the windage flanges fail to effectively reduce temperature within the coupling guard, and therefore cannot reduce the guard surface temperature. In addition, with the increase of radial clearance, there seems to exist a point (between 40 and 60mm) after which the windage flange has little affect on the temperature within the coupling guard, and the increasing negative pressure vacuum effect starts to decrease.

Analysis of Air Flow around Bolts

In an effort to explain the increase in temperature of the coupling flanges with windage flanges, the air flow around the bolt was analyzed. Figure 24 and Figure 25 show that there is no significant difference in the initial air flow separation at the drive bolts when windage flanges are present. The difference occurs after separation when the air travels around the bolt. The introduction of windage flanges shows that after separation the air is compressed between the bolt head and windage flange as it travels around the bolt. This can be seen to contribute to an increase in the temperature in this region by approximately 10°F (5°C). This behavior was found to be consistent on all guard configurations that were simulated, and is directly related to the coupling geometry.

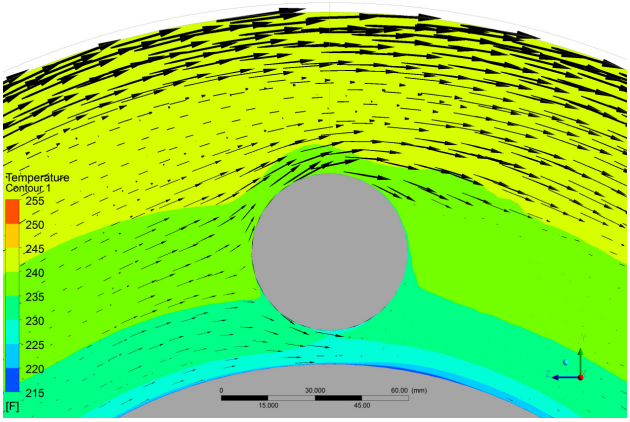

Figure 24. Flow Separation around Bolts with Temperature
Contour (Fluid Domain) on Medium Size Guard without Windage Flange

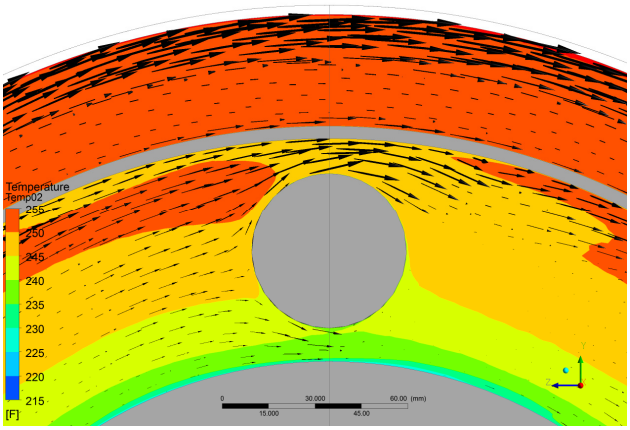

Figure 25. Flow Separation around Bolts with Temperature Contour (Fluid Domain) on Medium Size Guard with Windage Flange

Figure 26 and Figure 27 show that the heat generation is specifically related to an increased shear stress around the bolt surface, due to air being compressed through the gap, and also additional shear surface stress from addition of the windage geometry.

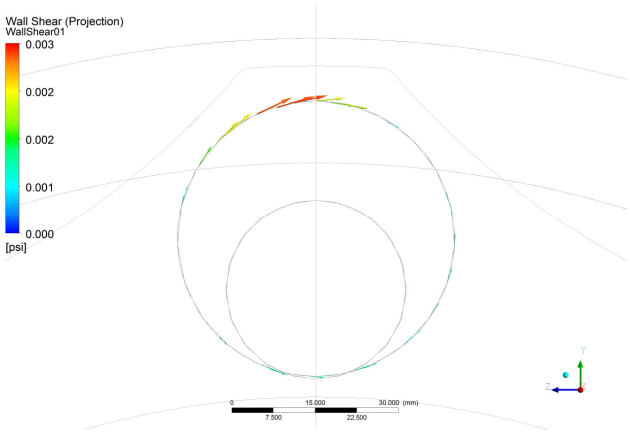

Figure 26. Shear Stress around Bolt on Medium Size Guard without Windage Flange Model

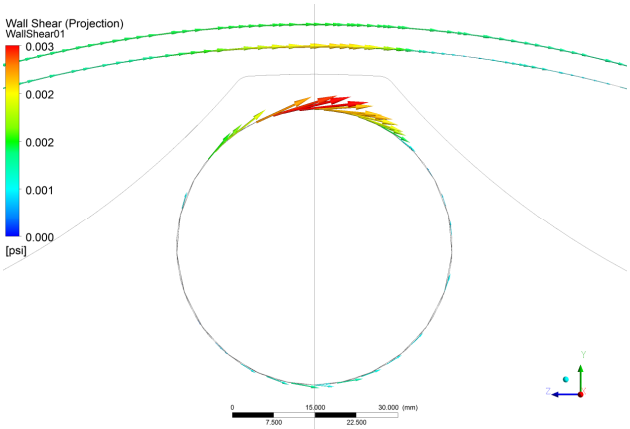

Figure 27. Shear Stress around Bolt and Windage Flange on Medium Size Guard with Windage Flange Model

The frictional torque on the inner guard face was plotted as shown in Figure 28, in order to establish how torque between the guard and large coupling OD is affected by the windage flange feature and radial guard clearance. It can be seen that on the small guard model, when the windage flange is introduced the torque greatly increases. The increase is smaller on the medium guard configuration and negligible on the large guard configuration. In addition, as the radial clearance increases, the frictional torque decreases. This shows that a small gap between the coupling OD and guard greatly increases the temperature generation at this point as a result of frictional torque, and that this is magnified by the presence of a windage flange. This however, is only true up to a certain point, after which the addition of a windage flange has no effect.

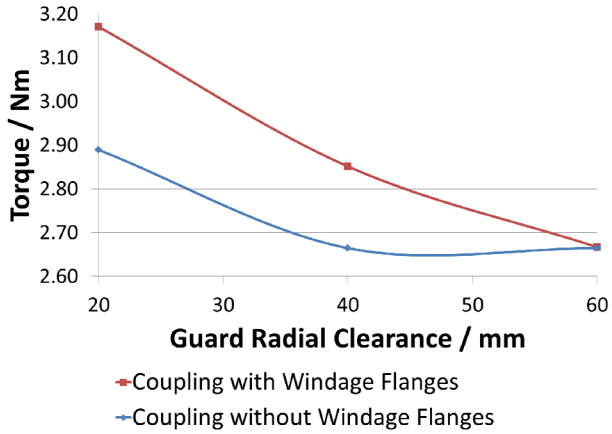

Figure 28. Frictional Torque on the Guard Inner-face with Test Coupling (with and without Windage Flanges) with different Guard Configuration Sizes

Coupling Heat Loss

Figure 29 shows that the introduction of the windage flange increases heat loss from the coupling. An increase in heat loss means that the coupling is generating more heat, which is an undesirable attribute as this is eventually transferred to the coupling guard. This supports the evidence above that the windage flanges specifically, contribute to the increased temperatures inside the guard.

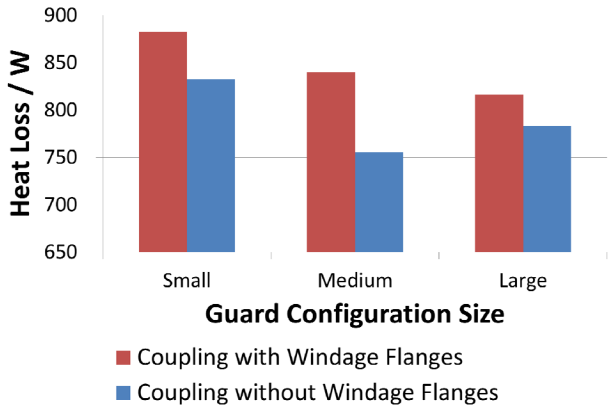

Figure 29. Heat Loss from the Test Coupling (with and without Windage Flanges) with different Guard Configuration Sizes

Guard Temperatures

Analysis of the maximum guard temperature (Figure 30), as expected, shows the same pattern of results as those for the temperature within the guard. Therefore, the conclusions drawn relating to the effect of radial guard clearance and the addition of windage features on temperature within the guard, are also true for guard surface temperature.

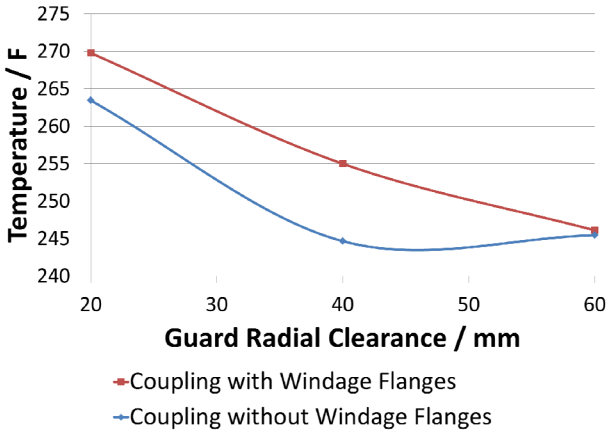

Figure 30. Guard Surface Temperature vs. Guard Radial Clearance

As heat loss is a function of area, it is fair to assume that the increase in guard surface area on larger guards contributes somewhat to the lower temperature that is found in the guard. Analyzing results for heat loss from the guard with increasing guard size, as shown in Figure 31, shows that when there is no windage flange the heat loss from the guard increases as the guard size increases. However, when the windage flange is present the heat loss from the guard can be seen to be high and therefore the change with increase guard size in negligible. This supports evidence discussed earlier, where when the radial clearance is small, the windage flanges result in increased frictional torque and subsequent heat generation between the large coupling OD and guard. This explains why with a small guard the heat loss is still high when windage flanges are present.

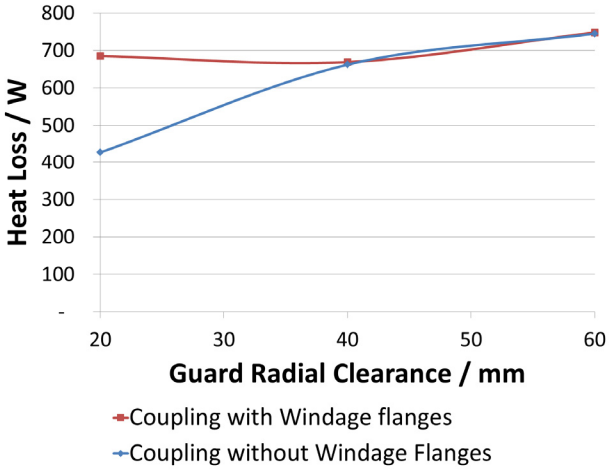

Figure 31. Guard Heat Loss vs. Guard Radial Clearance

CONCLUSIONS

Increasing guard radial clearance reduces temperature within the coupling guard. The main contributing factors to this are the increased heat losses experienced from larger guards due to the larger surface area, and improved air circulation within the guard leading to more evenly distributed temperature regions and no concentrated hot zones. However, this approach is less effective on couplings without windage flanges after a guard radial clearance of 40mm is reached ('break-even' point), when an increase in radial

clearance fails to reduce temperature any further.

Windage flanges fail to effectively reduce the temperature within coupling guards. Instead, the addition of windage flanges results in an increase of temperature within the guard. The increase in temperature is due to the windage flange introducing additional frictional torque. This was found to be the result of both the increased surface area from the windage flange geometry, and of air flow being compressed through the gap between the bolt head and windage flange. Again, as with the effect of radial clearance, this approach is less effective after the 'break-even' point is reached, after which the windage flange has a negligible effect on the temperature within the coupling guard. This was found to be due to small circulation patterns that are generated with windage geometry present on smaller radial guard clearances which have a reduced mixing capacity, dissipating with increased clearance. Determination of this critical point is important to maximize the cooling effect produced by increasing radial clearance and the effect of coupling windage features.

In addition, it was found that the phenomenon of negative pressure vacuum effect that is said to be present on large diameter couplings rotating at high speed was present in this study, in both CFD and physical results. As with the conclusions above, this was affected by the radial guard clearance 'break-even' point, where up to this point as radial guard clearance increased the negative pressure vacuum effect increased, after which it began to decrease again. This appears to be driven by a trade-off between two factors. As the guard radial clearance increases, this creates a larger diameter for the centrifuged air to flow around, increasing the vacuum effect. However, as a result, the larger diameter results in the coupling temperature having a weakening effect on inducing the air circulation cycle within the guard, reducing the vacuum effect.

The simulated results gained from CFD analysis were found to be very close to the experimental results (<4 percent) throughout the full temperature profile of the inner-guard. Correlation of simulated and experimental results on such commercial application to this level of accuracy is uncommon, and therefore the CFD approach adopted in this study should be utilized for future anti-windage or guard structure design, to validate other windage mitigation features and predict guard temperature.

REFERENCES

API 671, 2007, "Special Purpose Couplings for Petroleum, Chemical and Gas Industry Services," Fourth Edition, American Petroleum Institute, Washinton, D.C.

ASTM C1055-03, 2014, "Standard Guide for Heated System Surface Conditions that Produce Contact Burn Injuries", ASTM International, 100 Barr Harbor Drive, PO Box C700, West Conshohocken.

Bendix Corporation, 1982, Fluid Power Division, Catalog 67U-6-8211A.

Calisrat, M. M. and Munyon, R. E., 1985, "Design of Coupling Enclosures," *Proceedings of the Fourteenth Turbomachinery Symposium,* Turbomachinery Laboratory, Texas A&M University, College Station, Texas, pp. 51-57.

Calistrat, M. M., 1990, "Recent Case Histories with Coupling Enclosures," *Proceedings of the Nineteenth Turbomachinery Symposium,* Turbomachinery Laboratory, Texas A&M University, College Station, Texas, pp. 37-42.

Carter, D. Garvey, M. and Corcoran, J. P., 1994, "The Baffling and Temperature Prediction of Coupling Enclosures," *Proceedings of the Twenty-Third Turbomachinery Symposium*, Turbomachinery Laboratory, Texas A&M University, College Station, Texas, pp. 115-124.

Pennington, S. and Meck, K., 2012, "Effectiveness of Windage Features on High Speed Couplings," *Proceedings of the Forty First Turbomachinery Symposium*, Turbomachinery Laboratory, Texas A&M University, College Station, Texas

ACKNOWLEDGEMENTS

The authors would like to thank John Crane for allowing use of the dynamic test rig for physical testing, and for supporting and allowing them to publish and present this work. The authors also acknowledge technical support and funding provided by both John Crane Ltd. and the Texas A&M Turbomachinery Research Consortium (TRC).

